

A Search for $B^+ \rightarrow \tau^+ \nu_\tau$ Recoiling Against $B^- \rightarrow D^0 \ell^- \bar{\nu}_\ell X$

The BABAR Collaboration

March 22, 2003

Abstract

We present a search for the decay $B^+ \rightarrow \tau^+ \nu_\tau$ in 88.9×10^6 $\Upsilon(4S)$ decays recorded with the BABAR detector at the SLAC B -Factory. A sample of semi-exclusive, semi-leptonic B decays ($B^- \rightarrow D^0 \ell^- \bar{\nu}_\ell X$), where X is either a photon, π^0 , or nothing, is used to identify the daughter particles that are associated with the other B meson in each event. These particles are searched for evidence of a one-prong leptonic $B^+ \rightarrow \tau^+ \nu_\tau$ decay. For this data sample we set a preliminary upper limit on the branching fraction of $\mathcal{B}(B^+ \rightarrow \tau^+ \nu_\tau) < 4.9 \times 10^{-4}$ at the 90% confidence level. This result is then combined with a statistically independent BABAR search for $B^+ \rightarrow \tau^+ \nu_\tau$ to give a combined preliminary limit of $\mathcal{B}(B^+ \rightarrow \tau^+ \nu_\tau) < 4.1 \times 10^{-4}$.

Presented at the XXXVIIIth Rencontres de Moriond on
Electroweak Interactions and Unified Theories,
3/15—3/22/2003, Les Arcs, Savoie, France

Stanford Linear Accelerator Center, Stanford University, Stanford, CA 94309

Work supported in part by Department of Energy contract DE-AC03-76SF00515.

The BABAR Collaboration,

B. Aubert, R. Barate, D. Boutigny, J.-M. Gaillard, A. Hicheur, Y. Karyotakis, J. P. Lees, P. Robbe,
V. Tisserand, A. Zghiche

Laboratoire de Physique des Particules, F-74941 Annecy-le-Vieux, France

A. Palano, A. Pompili

Università di Bari, Dipartimento di Fisica and INFN, I-70126 Bari, Italy

J. C. Chen, N. D. Qi, G. Rong, P. Wang, Y. S. Zhu

Institute of High Energy Physics, Beijing 100039, China

G. Eigen, I. Ofte, B. Stugu

University of Bergen, Inst. of Physics, N-5007 Bergen, Norway

G. S. Abrams, A. W. Borgland, A. B. Breon, D. N. Brown, J. Button-Shafer, R. N. Cahn, E. Charles,
C. T. Day, M. S. Gill, A. V. Gritsan, Y. Groysman, R. G. Jacobsen, R. W. Kadel, J. Kadyk, L. T. Kerth,
Yu. G. Kolomensky, J. F. Kral, G. Kukartsev, C. LeClerc, M. E. Levi, G. Lynch, L. M. Mir, P. J. Oddone,
T. J. Orimoto, M. Pripstein, N. A. Roe, A. Romosan, M. T. Ronan, V. G. Shelkov, A. V. Telnov,
W. A. Wenzel

Lawrence Berkeley National Laboratory and University of California, Berkeley, CA 94720, USA

T. J. Harrison, C. M. Hawkes, D. J. Knowles, R. C. Penny, A. T. Watson, N. K. Watson

University of Birmingham, Birmingham, B15 2TT, United Kingdom

T. Deppermann, K. Goetzen, H. Koch, B. Lewandowski, M. Pelizaeus, K. Peters, H. Schmuecker,
M. Steinke

Ruhr Universität Bochum, Institut für Experimentalphysik 1, D-44780 Bochum, Germany

N. R. Barlow, W. Bhimji, J. T. Boyd, N. Chevalier, W. N. Cottingham, C. Mackay, F. F. Wilson

University of Bristol, Bristol BS8 1TL, United Kingdom

C. Hearty, T. S. Mattison, J. A. McKenna, D. Thiessen

University of British Columbia, Vancouver, BC, Canada V6T 1Z1

P. Kyberd, A. K. McKemey

Brunel University, Uxbridge, Middlesex UB8 3PH, United Kingdom

V. E. Blinov, A. D. Bukin, V. B. Golubev, V. N. Ivanchenko, E. A. Kravchenko, A. P. Onuchin,
S. I. Serebnyakov, Yu. I. Skovpen, E. P. Solodov, A. N. Yushkov

Budker Institute of Nuclear Physics, Novosibirsk 630090, Russia

D. Best, M. Chao, D. Kirkby, A. J. Lankford, M. Mandelkern, S. McMahon, R. K. Mommsen, W. Roethel,
D. P. Stoker

University of California at Irvine, Irvine, CA 92697, USA

C. Buchanan

University of California at Los Angeles, Los Angeles, CA 90024, USA

H. K. Hadavand, E. J. Hill, D. B. MacFarlane, H. P. Paar, Sh. Rahatlou, U. Schwanke, V. Sharma

University of California at San Diego, La Jolla, CA 92093, USA

J. W. Berryhill, C. Campagnari, B. Dahmes, N. Kuznetsova, S. L. Levy, O. Long, A. Lu, M. A. Mazur,
J. D. Richman, W. Verkerke

University of California at Santa Barbara, Santa Barbara, CA 93106, USA

J. Beringer, A. M. Eisner, C. A. Heusch, W. S. Lockman, T. Schalk, R. E. Schmitz, B. A. Schumm,
A. Seiden, M. Turri, W. Walkowiak, D. C. Williams, M. G. Wilson

University of California at Santa Cruz, Institute for Particle Physics, Santa Cruz, CA 95064, USA

J. Albert, E. Chen, M. P. Dorsten, G. P. Dubois-Felsmann, A. Dvoretzskii, D. G. Hitlin, I. Narsky,
F. C. Porter, A. Ryd, A. Samuel, S. Yang

California Institute of Technology, Pasadena, CA 91125, USA

S. Jayatileke, G. Mancinelli, B. T. Meadows, M. D. Sokoloff

University of Cincinnati, Cincinnati, OH 45221, USA

T. Barillari, F. Blanc, P. Bloom, P. J. Clark, W. T. Ford, U. Nauenberg, A. Olivas, P. Rankin, J. Roy,
J. G. Smith, W. C. van Hoek, L. Zhang

University of Colorado, Boulder, CO 80309, USA

J. L. Harton, T. Hu, A. Soffer, W. H. Toki, R. J. Wilson, J. Zhang

Colorado State University, Fort Collins, CO 80523, USA

D. Altenburg, T. Brandt, J. Brose, T. Colberg, M. Dickopp, R. S. Dubitzky, A. Hauke, H. M. Lacker,
E. Maly, R. Müller-Pfefferkorn, R. Nogowski, S. Otto, K. R. Schubert, R. Schwierz, B. Spaan, L. Wilden
Technische Universität Dresden, Institut für Kern- und Teilchenphysik, D-01062 Dresden, Germany

D. Bernard, G. R. Bonneaud, F. Brochard, J. Cohen-Tanugi, Ch. Thiebaux, G. Vasileiadis, M. Verderi

Ecole Polytechnique, LLR, F-91128 Palaiseau, France

A. Khan, D. Lavin, F. Muheim, S. Playfer, J. E. Swain, J. Tinslay

University of Edinburgh, Edinburgh EH9 3JZ, United Kingdom

C. Bozzi, L. Piemontese, A. Sarti

Università di Ferrara, Dipartimento di Fisica and INFN, I-44100 Ferrara, Italy

E. Treadwell

Florida A&M University, Tallahassee, FL 32307, USA

F. Anulli,¹ R. Baldini-Ferrolì, A. Calcaterra, R. de Sangro, D. Falciari, G. Finocchiaro, P. Patteri,
I. M. Peruzzi,¹ M. Piccolo, A. Zallo

Laboratori Nazionali di Frascati dell'INFN, I-00044 Frascati, Italy

A. Buzzo, R. Contri, G. Crosetti, M. Lo Vetere, M. Macri, M. R. Monge, S. Passaggio, F. C. Pastore,
C. Patrignani, E. Robutti, A. Santroni, S. Tosi

Università di Genova, Dipartimento di Fisica and INFN, I-16146 Genova, Italy

S. Bailey, M. Morii

Harvard University, Cambridge, MA 02138, USA

¹Also with Università di Perugia, Perugia, Italy

G. J. Grenier, S.-J. Lee, U. Mallik

University of Iowa, Iowa City, IA 52242, USA

J. Cochran, H. B. Crawley, J. Lamsa, W. T. Meyer, S. Prell, E. I. Rosenberg, J. Yi

Iowa State University, Ames, IA 50011-3160, USA

M. Davier, G. Grosdidier, A. Höcker, S. Laplace, F. Le Diberder, V. Lepeltier, A. M. Lutz, T. C. Petersen,
S. Plaszczynski, M. H. Schune, L. Tantot, G. Wormser

Laboratoire de l'Accélérateur Linéaire, F-91898 Orsay, France

R. M. Bionta, V. Brigljević, C. H. Cheng, D. J. Lange, D. M. Wright

Lawrence Livermore National Laboratory, Livermore, CA 94550, USA

A. J. Bevan, J. R. Fry, E. Gabathuler, R. Gamet, M. Kay, D. J. Payne, R. J. Sloane, C. Touramanis

University of Liverpool, Liverpool L69 3BX, United Kingdom

M. L. Aspinwall, D. A. Bowerman, P. D. Dauncey, U. Egede, I. Eschrich, G. W. Morton, J. A. Nash,
P. Sanders, G. P. Taylor

University of London, Imperial College, London, SW7 2BW, United Kingdom

J. J. Back, G. Bellodi, P. F. Harrison, H. W. Shorthouse, P. Strother, P. B. Vidal

Queen Mary, University of London, E1 4NS, United Kingdom

G. Cowan, H. U. Flaecher, S. George, M. G. Green, A. Kurup, C. E. Marker, T. R. McMahon, S. Ricciardi,
F. Salvatore, G. Vaitas, M. A. Winter

*University of London, Royal Holloway and Bedford New College, Egham, Surrey TW20 0EX,
United Kingdom*

D. Brown, C. L. Davis

University of Louisville, Louisville, KY 40292, USA

J. Allison, R. J. Barlow, A. C. Forti, P. A. Hart, F. Jackson, G. D. Lafferty, A. J. Lyon, J. H. Weatherall,
J. C. Williams

University of Manchester, Manchester M13 9PL, United Kingdom

A. Farbin, A. Jawahery, D. Kovalskyi, C. K. Lae, V. Lillard, D. A. Roberts

University of Maryland, College Park, MD 20742, USA

G. Blaylock, C. Dallapiccola, K. T. Flood, S. S. Hertzbach, R. Kofler, V. B. Koptchev, T. B. Moore,
H. Staengle, S. Willocq

University of Massachusetts, Amherst, MA 01003, USA

R. Cowan, G. Sciolla, F. Taylor, R. K. Yamamoto

Massachusetts Institute of Technology, Laboratory for Nuclear Science, Cambridge, MA 02139, USA

D. J. J. Mangeol, M. Milek, P. M. Patel

McGill University, Montréal, QC, Canada H3A 2T8

A. Lazzaro, F. Palombo

Università di Milano, Dipartimento di Fisica and INFN, I-20133 Milano, Italy

J. M. Bauer, L. Cremaldi, V. Eschenburg, R. Godang, R. Kroeger, J. Reidy, D. A. Sanders, D. J. Summers,
H. W. Zhao

University of Mississippi, University, MS 38677, USA

C. Hast, P. Taras

Université de Montréal, Laboratoire René J. A. Lévesque, Montréal, QC, Canada H3C 3J7

H. Nicholson

Mount Holyoke College, South Hadley, MA 01075, USA

C. Cartaro, N. Cavallo, G. De Nardo, F. Fabozzi,² C. Gatto, L. Lista, P. Paolucci, D. Piccolo, C. Sciacca
Università di Napoli Federico II, Dipartimento di Scienze Fisiche and INFN, I-80126, Napoli, Italy

M. A. Baak, G. Raven

*NIKHEF, National Institute for Nuclear Physics and High Energy Physics, 1009 DB Amsterdam,
The Netherlands*

J. M. LoSecco

University of Notre Dame, Notre Dame, IN 46556, USA

T. A. Gabriel

Oak Ridge National Laboratory, Oak Ridge, TN 37831, USA

B. Brau, T. Pulliam

Ohio State University, Columbus, OH 43210, USA

J. Brau, R. Frey, M. Iwasaki, C. T. Potter, N. B. Sinev, D. Strom, E. Torrence

University of Oregon, Eugene, OR 97403, USA

F. Colecchia, A. Dorigo, F. Galeazzi, M. Margoni, M. Morandin, M. Posocco, M. Rotondo, F. Simonetto,
R. Stroili, G. Tiozzo, C. Voci

Università di Padova, Dipartimento di Fisica and INFN, I-35131 Padova, Italy

M. Benayoun, H. Briand, J. Chauveau, P. David, Ch. de la Vaissière, L. Del Buono, O. Hamon,
Ph. Leruste, J. Ocariz, M. Pivk, L. Roos, J. Stark, S. T'Jampens

Universités Paris VI et VII, Lab de Physique Nucléaire H. E., F-75252 Paris, France

P. F. Manfredi, V. Re

Università di Pavia, Dipartimento di Elettronica and INFN, I-27100 Pavia, Italy

L. Gladney, Q. H. Guo, J. Panetta

University of Pennsylvania, Philadelphia, PA 19104, USA

C. Angelini, G. Batignani, S. Bettarini, M. Bondioli, F. Bucci, G. Calderini, M. Carpinelli, F. Forti,
M. A. Giorgi, A. Lusiani, G. Marchiori, F. Martinez-Vidal,³ M. Morganti, N. Neri, E. Paoloni, M. Rama,
G. Rizzo, F. Sandrelli, J. Walsh

Università di Pisa, Dipartimento di Fisica, Scuola Normale Superiore and INFN, I-56127 Pisa, Italy

²Also with Università della Basilicata, Potenza, Italy

³Also with IFIC, Instituto de Física Corpuscular, CSIC-Universidad de Valencia, Valencia, Spain

M. Haire, D. Judd, K. Paick, D. E. Wagoner
Prairie View A&M University, Prairie View, TX 77446, USA

N. Danielson, P. Elmer, C. Lu, V. Miftakov, J. Olsen, A. J. S. Smith, E. W. Varnes
Princeton University, Princeton, NJ 08544, USA

F. Bellini, G. Cavoto,⁴ D. del Re, R. Faccini,⁵ F. Ferrarotto, F. Ferroni, M. Gaspero, E. Leonardi,
M. A. Mazzoni, S. Morganti, M. Pierini, G. Piredda, F. Safai Tehrani, M. Serra, C. Voena
Università di Roma La Sapienza, Dipartimento di Fisica and INFN, I-00185 Roma, Italy

S. Christ, G. Wagner, R. Waldi
Universität Rostock, D-18051 Rostock, Germany

T. Adye, N. De Groot, B. Franek, N. I. Geddes, G. P. Gopal, E. O. Olaiya, S. M. Xella
Rutherford Appleton Laboratory, Chilton, Didcot, Oxon, OX11 0QX, United Kingdom

R. Aleksan, S. Emery, A. Gaidot, S. F. Ganzhur, P.-F. Giraud, G. Hamel de Monchenault, W. Kozanecki,
M. Langer, G. W. London, B. Mayer, G. Schott, G. Vasseur, Ch. Yeche, M. Zito
DAPNIA, Commissariat à l'Energie Atomique/Saclay, F-91191 Gif-sur-Yvette, France

M. V. Purohit, A. W. Weidemann, F. X. Yumiceva
University of South Carolina, Columbia, SC 29208, USA

D. Aston, R. Bartoldus, N. Berger, A. M. Boyarski, O. L. Buchmueller, M. R. Convery, D. P. Coupal,
D. Dong, J. Dorfan, D. Dujmic, W. Dunwoodie, R. C. Field, T. Glanzman, S. J. Gowdy, E. Grauges-Pous,
T. Hadig, V. Halyo, T. Hryn'ova, W. R. Innes, C. P. Jessop, M. H. Kelsey, P. Kim, M. L. Kocian,
U. Langenegger, D. W. G. S. Leith, S. Luitz, V. Luth, H. L. Lynch, H. Marsiske, S. Menke, R. Messner,
D. R. Muller, C. P. O'Grady, V. E. Ozcan, A. Perazzo, M. Perl, S. Petrak, B. N. Ratcliff, S. H. Robertson,
A. Roodman, A. A. Salnikov, R. H. Schindler, J. Schwiening, G. Simi, A. Snyder, A. Soha, J. Stelzer,
D. Su, M. K. Sullivan, H. A. Tanaka, J. Va'vra, S. R. Wagner, M. Weaver, A. J. R. Weinstein,
W. J. Wisniewski, D. H. Wright, C. C. Young
Stanford Linear Accelerator Center, Stanford, CA 94309, USA

P. R. Burchat, T. I. Meyer, C. Roat
Stanford University, Stanford, CA 94305-4060, USA

S. Ahmed, J. A. Ernst
State Univ. of New York, Albany, NY 12222, USA

W. Bugg, M. Krishnamurthy, S. M. Spanier
University of Tennessee, Knoxville, TN 37996, USA

R. Eckmann, H. Kim, J. L. Ritchie, R. F. Schwitters
University of Texas at Austin, Austin, TX 78712, USA

J. M. Izen, I. Kitayama, X. C. Lou, S. Ye
University of Texas at Dallas, Richardson, TX 75083, USA

⁴Also with Princeton University, Princeton, NJ 08544, USA

⁵Also with University of California at San Diego, La Jolla, CA 92093, USA

F. Bianchi, M. Bona, F. Gallo, D. Gamba

Università di Torino, Dipartimento di Fisica Sperimentale and INFN, I-10125 Torino, Italy

C. Borean, L. Bosisio, G. Della Ricca, S. Dittongo, S. Grancagnolo, L. Lanceri, P. Poropat,⁶ L. Vitale,
G. Vuagnin

Università di Trieste, Dipartimento di Fisica and INFN, I-34127 Trieste, Italy

R. S. Panvini

Vanderbilt University, Nashville, TN 37235, USA

Sw. Banerjee, C. M. Brown, D. Fortin, P. D. Jackson, R. Kowalewski, J. M. Roney

University of Victoria, Victoria, BC, Canada V8W 3P6

H. R. Band, S. Dasu, M. Datta, A. M. Eichenbaum, H. Hu, J. R. Johnson, R. Liu, F. Di Lodovico,
A. K. Mohapatra, Y. Pan, R. Prepost, S. J. Sekula, J. H. von Wimmersperg-Toeller, J. Wu, S. L. Wu, Z. Yu

University of Wisconsin, Madison, WI 53706, USA

H. Neal

Yale University, New Haven, CT 06511, USA

⁶Deceased

1 Introduction

In the Standard Model, the purely leptonic decay $B^+ \rightarrow \tau^+ \nu_\tau$ ¹ proceeds via quark annihilation into a W boson (Fig. 1). Its amplitude is thus proportional to the product of the B -decay constant, f_B and the quark-mixing-matrix element V_{ub} . The branching fraction is given by:

$$\mathcal{B}(B^+ \rightarrow \tau^+ \nu_\tau) = \frac{G_F^2 m_B m_\tau^2}{8\pi} \left[1 - \frac{m_\tau^2}{m_B^2} \right]^2 \tau_{B^+} f_B^2 |V_{ub}|^2, \quad (1)$$

where we have set $\hbar = c = 1$, G_F is the Fermi constant, V_{ub} is the quark mixing matrix element [2] [3], f_B is the B^+ meson decay constant, describing the overlap of the quark wave-functions inside the meson, τ_{B^+} is the B^+ lifetime and m_B and m_τ are the B^+ meson and τ masses. This expression is entirely analogous to that for pion decay. Physics beyond the Standard Model, such as SUSY, could enhance this process, as through the introduction of a charged Higgs [1].

Current theoretical values for f_B have large uncertainty, and purely leptonic decays of the B^+ meson may be the only clean experimental method of measuring f_B precisely. Given measurements of V_{ub} from semi-leptonic processes such as $B \rightarrow \pi \ell \nu$, f_B could be extracted from the measurement of the $B^+ \rightarrow \tau^+ \nu_\tau$ branching fraction. In addition, by combining the branching fraction measurement with results from B mixing the ratio $|V_{ub}|/|V_{td}|$ can be extracted from $\mathcal{B}(B^+ \rightarrow \tau^+ \nu_\tau)/\Delta m$, where Δm is the mass difference between the heavy and light neutral B meson states.

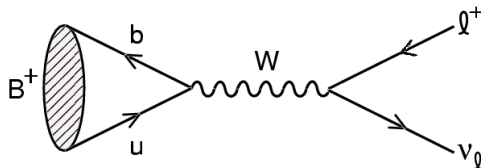


Figure 1: Purely leptonic B decay $B^+ \rightarrow \ell^+ \nu_\ell$ proceeds via quark annihilation into a W boson.

The decay amplitude is proportional to the lepton mass and decay to the lighter leptons is severely suppressed. This mode is thus the most promising for discovery at existing experiments. However, challenges such as the large missing momentum from several neutrinos make the signature for $B^+ \rightarrow \tau^+ \nu_\tau$ less distinctive than for other leptonic modes.

The Standard Model estimate of this branching fraction is 7.5×10^{-5} , given the PDG 2002 values for f_B , $|V_{ub}|$, and the B^+ lifetime: $f_B = 198 \text{ MeV}$, $V_{ub} = 0.0036$, $\tau_{B^+} = 1.674 \text{ ps}$ [4].

Purely leptonic B decays have not yet been observed. CLEO [5] and experiments at LEP [6][7][8] have searched for this process and set limits on the branching fraction at the 90% confidence level (CL). The most stringent limit on $\mathcal{B}(B^+ \rightarrow \tau^+ \nu_\tau)$ comes from the L3 experiment:

$$\mathcal{B}(B^+ \rightarrow \tau^+ \nu_\tau) < 5.7 \times 10^{-4} \text{ at the 90\% CL} \quad (2)$$

2 The BABAR Detector and Dataset

The data used in this analysis were collected with the *BABAR* detector at the PEP-II storage ring. The sample corresponds to an integrated luminosity of 81.9 fb^{-1} at the $\Upsilon(4S)$ resonance

¹Charge-conjugate modes are implied throughout this paper. The signal B will always be denoted as a B^+ decay while the semi-leptonic B will be denoted as a B^- to avoid confusion.

(on-resonance) and 9.58 fb^{-1} taken 40 MeV below the $\Upsilon(4S)$ resonance (off-resonance). The on-resonance sample consists of about 88.9 million $B\bar{B}$ pairs. The collider is operated with asymmetric beam energies, producing a boost of $\beta\gamma \approx 0.56$ of the $\Upsilon(4S)$ along the collision axis.

The *BABAR* detector is described elsewhere [9]. Charged-particle momentum, direction, and energy loss ($\frac{dE}{dx}$) measurements are performed by a five-layer double-sided silicon vertex tracker (SVT) and a 40-layer drift chamber (DCH) which are immersed in the field of a 1.5-T superconducting solenoid. Charged particle identification is performed by a detector of internally-reflected Cherenkov light (DIRC). The energies of electrons and photons are measured by the electromagnetic calorimeter (EMC) consisting of an array of 6580 CsI(Tl) crystals. The flux return is instrumented with resistive plate chambers (IFR) to detect the passage of muons and neutral hadrons.

A GEANT4-based [10] Monte Carlo (MC) simulation is used to model the signal efficiency and the physics backgrounds. Simulation samples equivalent to approximately three times the accumulated data were used to model $B\bar{B}$ events, and samples equivalent to approximately 1.5 times the accumulated data were used to model $e^+e^- \rightarrow u\bar{u}, d\bar{d}, s\bar{s}, c\bar{c}$, and $\tau^+\tau^-$ events.

3 Analysis Method

3.1 Event Selection

The decay $B^+ \rightarrow \tau^+\nu_\tau$ and subsequent one-prong leptonic decays $\tau^+ \rightarrow e^+\nu_e\bar{\nu}_\tau$ and $\tau^+ \rightarrow \mu^+\nu_\mu\bar{\nu}_\tau$ lead to the production of a single, visible charged particle and missing energy carried by neutrinos. Therefore, any remaining neutral energy or charged tracks originate from the other B . The search for $B^+ \rightarrow \tau^+\nu_\tau$ proceeds by reconstructing one of the B mesons in each event in the semi-leptonic topology $B^- \rightarrow D^0\ell^-\bar{\nu}_\ell X$ (henceforth referred to as the *semi-leptonic side* or *semi-leptonic B*), where X could be a photon, neutral pion, or nothing. The remainder of the event is searched for evidence of the one-prong leptonic τ^+ decay modes.

The choice of a semi-exclusive, semi-leptonic B decay means that the B meson cannot be fully reconstructed, since there is a neutrino missing and excited neutral D states are not reconstructed, potentially leaving unassigned neutral energy in the event. The inherent cleanliness of the events (small multiplicity, little unassigned neutral energy), however, is a powerful constraint that compensates for the choice of reconstruction mode. This method has been used in a search for $B^+ \rightarrow K^+\nu\bar{\nu}$ [11].

Events are pre-selected by requiring that their net charge is zero, that $R_2 < 0.9$ (where R_2 is the normalized second Fox-Wolfram moment [12]), and that they have large missing mass ($M_{miss} > 1.0 \text{ GeV}$). We select our semi-leptonic side by first reconstructing D^0 candidates in one of four modes: $D^0 \rightarrow K^-\pi^+$, $D^0 \rightarrow K^-\pi^+\pi^0$, $D^0 \rightarrow K^-\pi^+\pi^+\pi^-$, and $D^0 \rightarrow K_S^0\pi^+\pi^-$. The K_S^0 is reconstructed only in the charged mode $K_S^0 \rightarrow \pi^+\pi^-$. The D^0 meson is required to have a momentum in the center-of-mass ($\Upsilon(4S)$) frame $p_{D^0}^* > 0.5 \text{ GeV}$, and its daughters are required to meet particle identification criteria consistent with the particle hypothesis.

We pair the D^0 candidates with leptons whose momentum in the center-of-mass frame meets the requirement $p_\ell^* > 1.3 \text{ GeV}$. The D^0 -lepton pairs are required to converge at a common vertex; these pairs are referred to as $D\ell$ candidates. If there are multiple $D\ell$ candidates in an event we select the candidate whose reconstructed D^0 mass is closest to the average reconstructed mass for its decay mode. If the best candidate can be paired with a pion to make a $D^{*+}\ell^-$ candidate, then the event is consistent with being a $B^0\bar{B}^0$ event and is rejected.

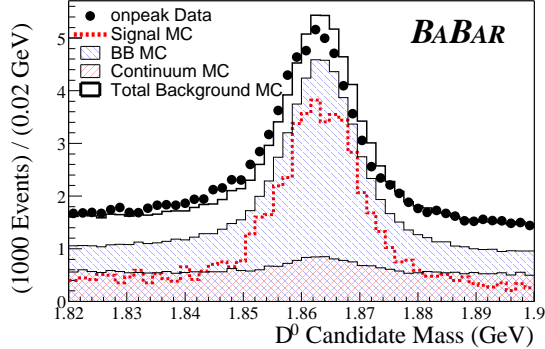


Figure 2: The D^0 mass distribution after making event preselections and requiring that events have at least one $B^- \rightarrow D^0 \ell^- \bar{\nu}_\ell X$ candidate. Background MC combines $B\bar{B}$ (excluding $B^+ \rightarrow \tau^+ \nu_\tau$ decays) and continuum MC and is normalized to the data area, while the normalization of the signal simulation is arbitrary. Due to the large size of this sample, the data error bars are too small to see in the figure.

The mass distribution for these D^0 candidates is shown in Fig. 2. There is a difference between the mean of data and the mean of MC because the MC generator uses a D^0 mass that differs from the PDG value by 1 MeV. The width of distribution is typically narrower in MC by 0.2 MeV ($K^- \pi^+$) to 4 MeV ($K^- \pi^+ \pi^0$) due to energy and momentum resolution differences in data and MC. To account for differences in mean position and peak width, we require that the reconstructed D^0 mass be within 3σ of the fitted mean for the mode under consideration. The widths of the peaks vary by D^0 mode, from 3.8 MeV for $D^0 \rightarrow K^- \pi^+ \pi^- \pi^+$ to 10.4 MeV for $D^0 \rightarrow K^- \pi^+ \pi^0$.

A restriction is also placed on $\cos \theta_{B,D\ell}$, where $\theta_{B,D\ell}$ is computed from B and $D\ell$ momenta and energy in the center-of-mass frame under the assumption that only a neutrino is missing,

$$\cos \theta_{B,D\ell} = \frac{(2 E_B E_{D\ell} - m_B^2 - m_{D\ell}^2)}{2 |\vec{p}_B| |\vec{p}_{D\ell}|}. \quad (3)$$

Since the semi-leptonic B cannot be completely reconstructed its energy, E_B , and momentum, $|\vec{p}_B|$, are derived from the beam energies. The variable $\cos \theta_{B,D\ell}$ can take on values outside $(-1, 1)$ for events in which particles besides the neutrino have been missed in the semi-leptonic decay. We allow for the feed-down of excited neutral D states into the analysis by applying an asymmetric cut of $-2.5 < \cos \theta_{B,D\ell} < 1.1$. This variable is shown in Fig. 3. Differences in the semi-leptonic side between data and simulation are later corrected (Sec. 4.2) in the overall efficiency estimate.

Once the semi-leptonic side has been reconstructed, its daughter particles are excluded from the event. Any neutral or charged object that is not associated with the semi-leptonic side is referred to as belonging to the *signal side*. The event is then required to have only one remaining charged particle with a small impact parameter in the (r, ϕ) plane. This track is required to fail kaon identification and be identified either as a muon or an electron. In addition, $\tau^+ \tau^-$ continuum events are rejected by making requirements on the angle of the track with respect to the event thrust axis ($|\cos \theta_{\vec{p}, \vec{T}}| < 0.9$) and the minimum mass capable of being made from any three tracks in the event ($M_3^{min} > 1.5 \text{ GeV}$). In general, continuum events are sharply peaked toward 1.0 in $|\cos \theta_{\vec{p}, \vec{T}}|$; additionally, $\tau^+ \tau^-$ events tend to have a value of M_3^{min} peaked below the τ mass.

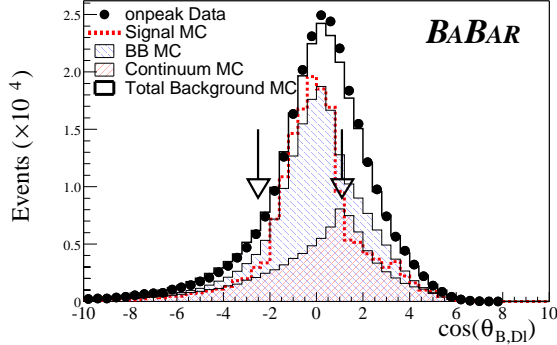


Figure 3: The quantity $\cos\theta_{B,D\ell}$, computed from the energies and momenta of the $D\ell$ and the B meson assuming only a neutrino is missing. Background MC combines $B\bar{B}$ (excluding $B^+ \rightarrow \tau^+\nu_\tau$ decays) and continuum MC and is normalized to the data area, while the normalization of the signal simulation is arbitrary. The arrows represent the boundaries of the selection region between -2.5 and 1.1 . Due to the large size of this sample, the data error bars are too small to see in the figure.

The variable E_{left} , the neutral energy remaining in the calorimeter after excluding neutrals from the semi-leptonic B , provides good discrimination between signal and background (Fig. 4). For true signal events, this quantity is peaked toward zero energy while for background it peaks near 2 GeV. We make a loose restriction of $E_{\text{left}} < 1.0$ GeV in preparation for the final step of the analysis, which is to fit the E_{left} distribution and extract the signal and background contributions.

To minimize experimenter bias, the data were not studied in the signal-populated region of E_{left} until systematic checks were performed using control samples in the region of E_{left} ($E_{\text{left}} > 0.5$ GeV) which does not contain a significant signal yield. The region $0.5 < E_{\text{left}} < 1.0$ GeV is defined to be the *neutral energy sideband*, while the region $E_{\text{left}} < 0.5$ GeV is referred to as the *signal region*.

3.2 Selection Efficiency

After applying all selection criteria we obtain a signal efficiency in the Monte Carlo simulation of $(6.99 \pm 0.31) \times 10^{-4}$, where the error is purely from the statistics of the signal MC. This number does not include corrections for differences between data and simulation, which will be described in Sec. 4. The number of background events expected for $E_{\text{left}} < 1.0$ GeV, determined from simulation, is 269.1 ± 9.6 , where the error is purely statistical.

3.3 The Limit-Setting Procedure

We fit E_{left} using an extended maximum likelihood function; from this fit we extract the contributions to the distribution from signal and background events. The likelihood function is of the following form:

$$\mathcal{L} = e^{-(\mu_s + \mu_b)} \prod_{i=1}^n (\mu_s F_s(E_{\text{left}i}) + \mu_b F_b(E_{\text{left}i})) \quad (4)$$

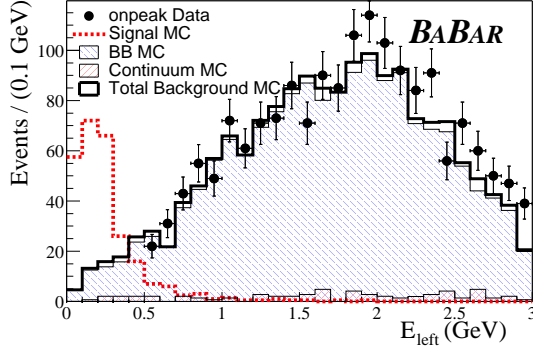


Figure 4: E_{left} , the neutral energy remaining in the calorimeter after excluding neutrals associated with the semi-leptonic side. In the above distribution all analysis selection criteria are applied. The data are not shown below 0.5 GeV. The normalization of the signal MC is arbitrary.

where μ_s is the number of signal events, μ_b is the number of background events (both of which are obtained by fitting the selected data sample) and n is the total number of events in the selected sample. The functions $F_s(E_{\text{left}})$ and $F_b(E_{\text{left}})$ are the Probability Density Functions (PDFs) which are obtained from the E_{left} distributions in signal and background MC. The *nominal* models for signal and background are shown in Fig. 5.

The E_{left} distribution in the signal MC has several salient features. The peak at 200 MeV arises from the unassigned photon or π^0 daughter of a D^{*0} on the semi-leptonic side. The peak at zero energy arises from events without remaining neutral energy, and above zero the spectrum falls exponentially under the peak from the D^{*0} neutrals, the result of neutrals in the MC arising from beam background and hadronic split-offs.

The background PDF is a second-order polynomial rising monotonically between 0 GeV and 1.0 GeV. An estimate of the background from data is determined by extrapolating the data E_{left} sideband into the signal region using the background PDF. The result is a background estimate of 273.6 ± 19.2 events.

To determine the 90% confidence limit, denoted μ_s^{90} , for the measured value of μ_s we use a modified frequentist approach based on that used by the LEP experiments in the Higgs search [14]. This approach constructs an estimator based on the fitted signal yield, μ_s^{fitted} . In all following discussions, *toy MC* refers to E_{left} spectra obtained by randomly sampling the signal and background E_{left} PDFs and treating the samples as a data set. The limit-setting method is outlined as follows:

1. Toy MC experiments are generated with our expected number of background events and a signal hypothesis, $\mu_s^{\text{input}} = \mu_s^{\text{expected}}$. Each toy experiment is fitted for the signal yield, μ'_s . The collection of μ'_s forms a distribution. We denote the normalized fitted signal distribution for the original signal hypothesis as $D_{s+b}(\mu'_s, \mu_s^{\text{input}})$.
2. Toy MC is also generated with a signal hypothesis of zero events and with the expected number of background events. Again, each data sample is fitted and we obtain the distribution of the fitted signal yield. We denote the normalized distribution of the fitted signal yield in the null signal hypothesis as $D_b(\mu'_s)$.
3. For a specific data sample, a fit is performed using the likelihood function to obtain the number

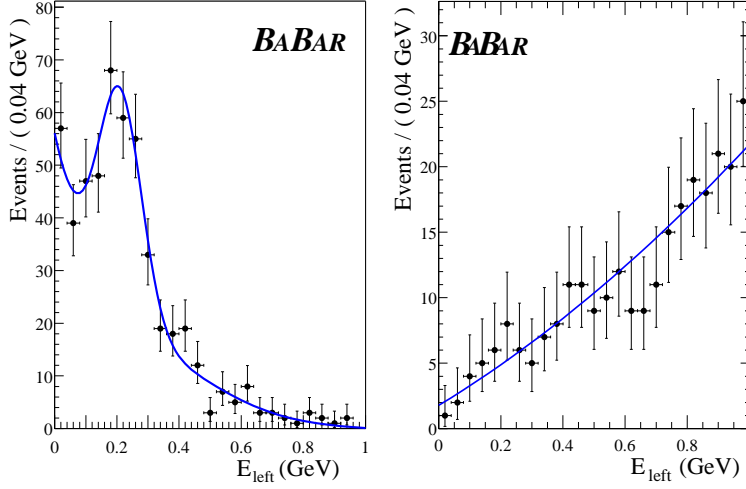


Figure 5: The signal PDF (left) fitted to E_{left} from the signal MC and the background PDF (right) fitted to E_{left} from the background MC. All selection criteria are applied to the events in signal and background MC. The normalization of the signal MC is arbitrary and the normalization of the background MC is fixed to the integrated luminosity.

of signal events in the sample, μ_s^{fitted} . The confidence level (CL) for this measurement, for a signal hypothesis μ_s^{expected} , is given by:

$$CL(\mu_s^{\text{fitted}}, \mu_s^{\text{expected}}) \equiv \frac{\int_{-\infty}^{\mu_s^{\text{fitted}}} D_{s+b}(\mu'_s; \mu_s^{\text{expected}}) d\mu'_s}{\int_{-\infty}^{\mu_s^{\text{fitted}}} D_b(\mu'_s) d\mu'_s} \quad (5)$$

4. The 90% confidence limit corresponding to this fitted signal yield, μ_s^{fitted} , is defined by the requirement:

$$CL(\mu_s^{\text{fitted}}, \mu_s^{90}) = 1 - 0.90 \quad (6)$$

A scan is performed over signal hypotheses until the minimum signal hypothesis which satisfies the requirement is determined. This signal hypothesis is μ_s^{90} . The relationship between μ_s^{90} and μ_s^{fitted} is given in Fig. 6.

We use the background-only hypothesis to determine the nominal sensitivity for the analysis. The nominal background PDF is used to generate 10,000 toy MC experiments, each with a total number of events Poisson-distributed around the nominal background expectation of 269 ± 9.6 events. The E_{left} distribution so generated for each experiment is fitted with the likelihood function, and the curve in Fig. 6 is used to obtain the corresponding μ_s^{90} . The distribution of μ_s^{90} for these toy experiments is shown in Fig. 6, and the median of this distribution provides our nominal sensitivity, $\mu_s^{90} = 15.4$.

A test of the method is performed using two independent samples of GEANT4 MC, each with a total luminosity equal to that of the data set. Each simulated experiment contains only background

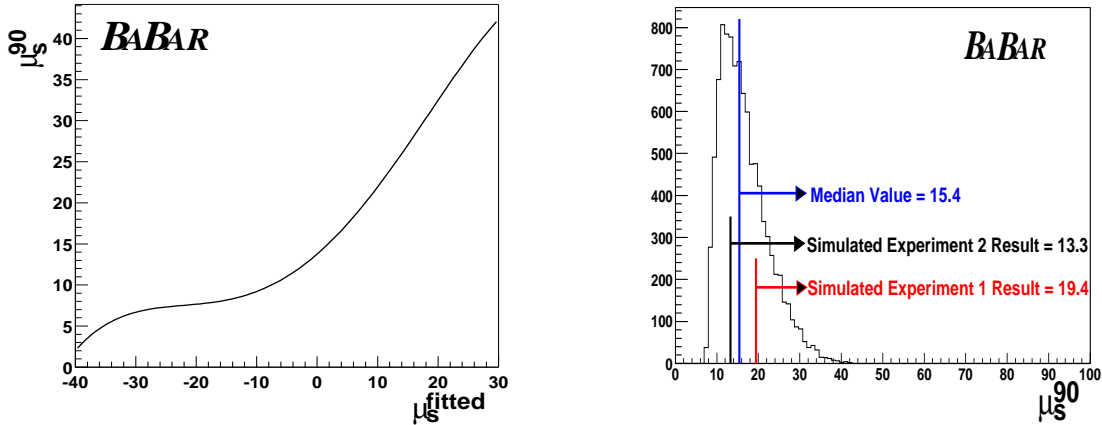


Figure 6: The relationship between μ_s^{90} and μ_s^{fitted} is shown in the left figure. In the right figure is the distribution of μ_s^{90} obtained from fitting 10,000 toy MC experiments generated using the null signal hypothesis. The black line indicates the median of this distribution, which is taken as the nominal sensitivity of the analysis ($\mu_s^{90} = 15.4$). The red and blue lines indicate the results of applying the analysis to two independent, background-only GEANT4 MC experiments.

events and has all analysis selection criteria applied. The results obtained from fitting these two experiments, $\mu_s^{90} = 13.3$ and $\mu_s^{90} = 19.4$ are in good agreement with the nominal sensitivity and are illustrated in Fig. 6. The results of these GEANT4 MC experiments are used in Sec. 4.1 to explore potential systematic effects on the limit-setting procedure.

The strength of this method is that it takes full advantage of the information contained in the shape of the signal and background and is insensitive to the absolute background normalization. It relies on the accuracy of the simulation, in particular the simulation of the calorimeter for low neutral cluster energy. The systematic effects on the limit-setting procedure, as well as on the signal efficiency, are discussed in the next section.

4 Evaluation of Systematic Uncertainties

In this section we discuss the systematic uncertainties affecting the limit-setting procedure and the calculation of the efficiency.

4.1 Systematic Effects for Limit-Setting

Table 1 lists the sources of systematic uncertainty and their effects on the overall expected sensitivity of a pair of independent “experiments” derived from the background MC sample. Since MC is used to generate the PDFs for signal and background, effects of concern are those which might cause the true background or signal distributions to differ from the simulation. For each source of potential systematic uncertainty listed below, a CL curve is calculated (as in Fig. 6) by generating toy MC with a systematically modified model and fitting with the nominal model.

To explore the potential differences between data and MC when validating the background

PDF, several control samples have been developed by performing the semi-leptonic reconstruction on data and MC and applying selection criteria to the remainder of the event:

- $(B^- \rightarrow D^0 \ell^- \bar{\nu}_\ell X) + (\text{anything})$: The $B^- \rightarrow D^0 \ell^- \bar{\nu}_\ell X$ reconstruction algorithm is applied and no restrictions are placed on the signal side.
- $(B^0 \rightarrow D^{*+} \ell^- \nu) + (\mathbf{1 \ track})$: The semi-leptonic reconstruction algorithm is applied, but semi-leptonic candidates are kept where the best candidate is reconstructed as a $D^{*+} \ell^- \nu$. We then require only one track remaining in the event. This sample has a topology similar to the signal sample.
- $(B^- \rightarrow D^0 \ell^- \bar{\nu}_\ell X) + (\mathbf{2 \ tracks})$: The $B^- \rightarrow D^0 \ell^- \bar{\nu}_\ell X$ reconstruction algorithm is applied and the signal side is required to contain exactly two charged tracks. This requirement enforces a mis-reconstructed signal side, since total event charge is non-zero.

The difference between data and simulation for each of these samples is used to construct a correction function for the PDFs. The PDFs are multiplied by the correction function and re-normalized. The upper limit is recalculated using the corrected PDFs to generate the toy MC samples discussed in Sec. 3, while fitting is still performed with the nominal model. The results of this study are given in Table 1.

Motivated by the data/MC yield disagreement in the control samples, we explored the effects of a significant difference between the actual background and the background expectation. Given the expected background from MC (269.1 ± 9.6 events), we varied the input background hypothesis to our toy MC by ± 10 and ± 20 events and used the nominal likelihood function to generate CL curves for each case. The result was a change in the nominal sensitivity of μ_s^{90} of no more than 0.5 events (Table 1). Therefore we concluded that if the actual background in data is different than the expectation from MC, the resulting change in the limit is small.

The choice of background parametrization has also been explored as a possible effect on the limit-setting procedure. Different models (second-order polynomial, Gaussian tail, KEYS [13], histogram) were used to represent the background E_{left} spectrum and then generate toy MC. These toy samples were again fitted with the nominal model and the variation in the confidence limit curve was explored. The results are given in Table 1. Limit curves calculated from this variation in the background model yielded a lower limit on the signal yield, suggesting that the second-order polynomial leads to a conservative limit.

A feature at or near zero energy in the E_{left} spectrum, unmodelled in the Monte Carlo, is another possible effect in the background that could fake a signal. Such a feature is suggested by studying the $B^0 \rightarrow D^{*+} \ell^- \nu + 1 \text{ track}$ control sample, which suggested a maximal difference near zero energy in data and MC of a factor of two. To explore the effect of such a feature, toy MC is generated with the background PDF enhanced by a factor of two near zero. This toy MC is then fit using the nominal signal and background models to study the variation in the confidence limit. The results are given in Table 1.

To validate the signal PDF, a control sample of $B^- \rightarrow D^0 \ell^- \bar{\nu}_\ell X, B^+ \rightarrow \bar{D}^{*0} \ell^+ \nu_\ell$ is used to check the difference between data and simulation after making all semi-leptonic and signal-side requirements. This sample has a semi-leptonic side as in the signal analysis, and a signal side which is also reconstructed as an independent $B^+ \rightarrow \bar{D}^0 \ell^+ \nu_\ell X$. We then construct a subsample of these events where a photon or π^0 could be associated with the \bar{D}^0 on the signal side to make a \bar{D}^{*0} . Having attempted to account for the neutral from \bar{D}^{*0} decay on the signal side, the neutral

energy spectrum should resemble that for signal events. However, this subsample has more neutral energy present from hadronic splitoffs, and the correct photon or π^0 is not always associated with the \bar{D}^0 to make the \bar{D}^{*0} . Therefore, a comparison is made between data and the corresponding MC sample and not between data and signal MC. The sample suggests that there may be a difference of ~ 20 MeV in the overall position of the peak near 200 MeV. The effects of such a difference are given in Table 1.

Table 1: Sources of potential systematic uncertainty have been explored and their effects on the expectation for μ_s^{90} observed. The simulated experiments come from two independent samples of full MC, each with luminosity equivalent to the data luminosity. Despite the many potential differences between data and simulation, the variation in the upper limit is small compared to the variation of limit expected for the zero signal hypothesis.

Systematic Variation	Control Sample used to guide the variation	μ_s^{90} Simulated Experiment 1	μ_s^{90} Simulated Experiment 2
None (Nominal Model)	None	19.4	13.3
Data/Simulation Shape Difference	$B^- \rightarrow D^0 \ell^- \bar{\nu}_\ell X$ + anything $B^0 \rightarrow D^{*+} \ell^- \nu$ + 1 track $B^- \rightarrow D^0 \ell^- \bar{\nu}_\ell X$ + 2 tracks	18.0 18.6 17.8	12.4 13.0 12.2
Incorrect Background Estimate	All	-20 Events	12.0
-10 Events		19.0	13.1
+10 Events		19.3	13.6
+20 Events		19.7	13.7
		19.8	
Gaussian Tail Background Model	None	17.1	12.0
KEYS Background Model	None	17.4	12.0
Histogram Background Model	None	17.2	11.8
Factor of 2 enhancement in background near $E_{\text{left}} = 0.0$ GeV	$B^0 \rightarrow D^{*+} \ell^- \nu$ + 1 track	16.5	11.5
+20 MeV Shift in Signal PDF Gaussian	$B^- \rightarrow D^0 \ell^- \bar{\nu}_\ell X, B^+ \rightarrow \bar{D}^{*0} \ell^+ \nu_\ell$	20.2	13.9
-20 MeV Shift in Signal PDF Gaussian	$B^- \rightarrow D^0 \ell^- \bar{\nu}_\ell X, B^+ \rightarrow \bar{D}^{*0} \ell^+ \nu_\ell$	18.9	13.0

In almost all cases that were investigated, the nominal model yields the most conservative CL curve. Additionally, the variation in the upper limit expectation is small compared to the overall variation of the limit for the zero signal hypothesis. We therefore use the nominal model to set the limit, having determined that the systematic effects mentioned above have negligible impact on the result.

Table 2: The corrections which are applied in this analysis on the signal efficiency, as well as the error associated with each correction.

Source	Correction Factor	Correction Error
B-Counting	1.0	0.011
Semi-Leptonic Reconstruction Efficiency	0.958	0.051
Neutral Energy	1.0	0.025
Tracking Efficiency (signal track only)	1.0	0.008
Particle ID (signal track only)	0.836	0.042
Total	0.801	0.063

4.2 Systematic Effects for Signal Efficiency

The efficiency calculated in Sec. 3.2 needs to be corrected for differences in data and MC. The effects of several systematic uncertainty have been evaluated. The results are expressed in a correction factor and a systematic error associated with the correction. The most prominent sources of systematic uncertainties are listed in Table 2.

The semi-leptonic reconstruction efficiency correction is evaluated by using a sample of N_2 double-reconstruction events ($B^- \rightarrow D^0 \ell^- \bar{\nu}_\ell X$, $B^+ \rightarrow \bar{D}^0 \ell^+ \nu_\ell X$) and a sample of N_1 single-reconstruction events in the same data set, where the single-reconstruction sample excludes double-reconstructed events. To isolate the effects of the semi-leptonic reconstruction, we remove the event preselection requirements which are unrelated to the selection of the semi-leptonic decay. The ratio of the sizes of these two samples is given by:

$$\frac{N_1}{N_2} = \frac{2(1 - \varepsilon)}{\varepsilon} \quad (7)$$

where ε is the probability of selecting a second B meson in the mode $B^- \rightarrow D^0 \ell^- \bar{\nu}_\ell X$ having already selected one B meson in that mode. Equation 7 is solved for ε , and the ratio of ε in data and simulation is taken as a correction on the efficiency,

$$\frac{\varepsilon_{data}}{\varepsilon_{MC}} = 0.958 \pm 0.051. \quad (8)$$

The correction of the signal efficiency due to particle identification (PID) is performed as follows. Using control samples of electrons and muons from data, the performance of the kaon veto and lepton identification is evaluated as a function of lab momentum (p) and polar angle (θ). This performance translates into a weight for an identified track with a given momentum. Integrating this weight over the momentum spectrum of the signal MC for true one-prong leptonic τ^+ decays provides the efficiency of the selection in data.

The efficiency in the MC is evaluated by comparing the true identity of a τ^+ daughter to the reconstructed identity. The ratio of the data efficiency to the MC efficiency is taken as the signal efficiency correction from particle identification. The statistical uncertainties on the signal MC

sample size and PID weights translate into a systematic error on the correction. This error is dominated by the signal MC sample size.

We apply the total correction listed in Table 2 to the signal efficiency from MC to obtain the signal efficiency, $(5.60 \pm 0.25(stat.) \pm 0.44(syst.)) \times 10^{-4}$. The uncertainty on each correction is propagated through to a systematic error on the signal efficiency, while the statistical uncertainty derives from the signal MC sample size.

Systematic uncertainty is incorporated into the branching fraction limit as follows: for each branching fraction hypothesis, the corresponding signal hypothesis is determined by sampling 10,000 times from a Gaussian distribution about the mean of the signal efficiency, where the width of the Gaussian is given by the systematic error on the signal efficiency. From each signal hypothesis a toy MC experiment is generated and fitted using the likelihood function. This is repeated for many branching fraction hypotheses and the CL curve, including systematic error, is calculated.

5 Results

We apply all selection criteria in the analysis and fit the E_{left} spectrum in the data below 1.0 GeV using the nominal likelihood function. The result of the fit is given in Table 3 and shown in Fig. 7.

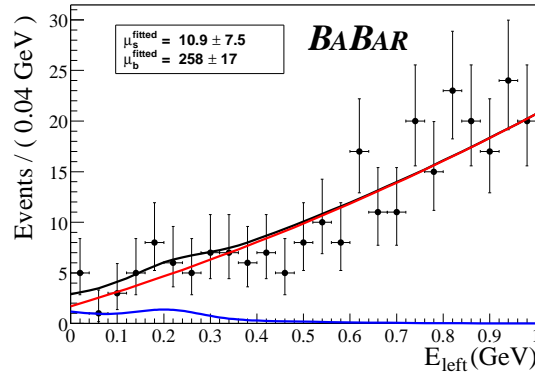


Figure 7: The E_{left} spectrum in data from zero to 1.0 GeV and the fit of the likelihood function to the spectrum.

Table 3: The results of the fit of the likelihood function to data is given below.

Fit Parameter	Fitted Value
μ_s^{fitted}	10.9 ± 7.5
μ_b^{fitted}	258 ± 17

The background yield of 258 ± 17 is in agreement with the expectation from extrapolating sideband data into the E_{left} signal region, 274 ± 19 .

We apply our confidence limit curve to the fitted number of signal events (Fig. 6) and determine

the 90% confidence limit on the signal yield to be

$$\mu_s^{90} = 22.8, \tag{9}$$

which yields a limit on the branching fraction at the 90% confidence level of

$$\mathcal{B}(B^+ \rightarrow \tau^+ \nu_\tau) < 4.6 \times 10^{-4} \text{ at the 90\% CL} \tag{10}$$

where we have assumed equal production of B^+B^- and $B^0\bar{B}^0$ at the $\Upsilon(4S)$ resonance. The expectation from studies in MC containing zero signal events was given in Sec. 3 as $\mu_s^{90} = 15.4$; the comparison of the expected sensitivity and the measured result is shown in Fig. 8.

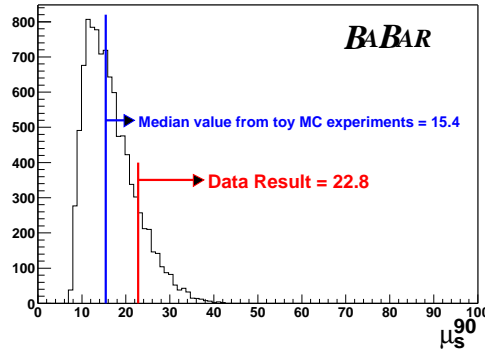


Figure 8: The nominal sensitivity (15.4), obtained from the median of 10,000 toy MC experiments, is compared to the result from data (22.8).

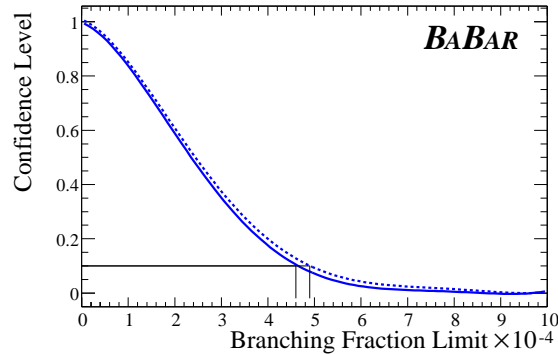


Figure 9: The relationship between the confidence level and the branching fraction limit both in the case where systematic error is (dashed) and is not (solid) incorporated. Lines are drawn at the locations of the 90% confidence limits for both cases.

After incorporating the systematic uncertainty on the signal efficiency (Fig. 9) we find an upper limit on the branching fraction of

$$\mathcal{B}(B^+ \rightarrow \tau^+ \nu_\tau) < 4.9 \times 10^{-4} \text{ at the 90\% CL} \tag{11}$$

A separate *BABAR* analysis to search for $B^+ \rightarrow \tau^+ \nu_\tau$ has also been performed where B mesons are reconstructed via the semi-exclusive hadronic modes $B^- \rightarrow D^{(*)0} X^-$, where X^- represents a combination of up to five charged pions or kaons and up to two π^0 candidates. The semi-exclusive hadronic reconstruction analysis is statistically independent of the present work and has obtained the limit [15]

$$\mathcal{B}(B^+ \rightarrow \tau^+ \nu_\tau) < 7.7 \times 10^{-4} \text{ at the 90\% CL} \quad (12)$$

The results of this statistically independent analysis are combined with that reported here using the same modified frequentist method. For each analysis, 5000 toy MC experiments are generated each for a branching fraction hypothesis between 1×10^{-4} and 10×10^{-4} in steps of 2.5×10^{-6} . The number of events in each toy experiment that contains signal and background is denoted $n_{(s+b)}$. For each branching fraction hypothesis a separate sample of 5000 background-only toy experiments is also generated; the number of events in a given experiment in this sample is denoted $n_{(b)}$. For a given hypothesis i (where $i = (s+b)$, (b) , or *data*) the likelihood estimators, Q_i , are calculated in each toy experiment:

$$Q_i = \frac{\mathcal{L}(n_i|s+b)}{\mathcal{L}(n_i|b)} \quad (13)$$

where $\mathcal{L}(n_i|s+b)$ is the likelihood of a given toy experiment with n_i events being consistent with the $(s+b)$ hypothesis (in equation 4, μ_s is set to the number of signal s , corresponding to the branching fraction hypothesis, and μ_b is set to the number of background b). Systematic errors are incorporated by each analysis into the Q_i . They are combined as follows:

$$Q_i^{\text{combined}} = Q_i^{\text{semi-leptonic}} \times Q_i^{\text{hadronic}}. \quad (14)$$

The confidence level for a particular branching ratio hypothesis is given by counting the number of experiments, $N_{(Q_i < Q_{data})}$, that have a value of $Q_{(s+b)}$ ($Q_{(b)}$) less than that for data (Q_{data}) and taking the ratio

$$CL_s = \frac{N_{(Q_{(s+b)} < Q_{data})}}{N_{(Q_{(b)} < Q_{data})}}. \quad (15)$$

From this a combined *BABAR* result is obtained:

$$\mathcal{B}(B^+ \rightarrow \tau^+ \nu_\tau)_{\text{combined}} < 4.1 \times 10^{-4} \text{ at the 90\% CL.} \quad (16)$$

6 Summary

We have performed a search for the decay process $B^+ \rightarrow \tau^+ \nu_\tau$. To accomplish this a sample of semi-leptonic B decays ($B^- \rightarrow D^0 \ell^- \bar{\nu}_\ell X$) has been used to reconstruct one of the B mesons and the remaining information in the event is searched for evidence of $B^+ \rightarrow \tau^+ \nu_\tau$. We find no evidence for this decay process and set a preliminary limit on its branching fraction of

$$\mathcal{B}(B^+ \rightarrow \tau^+ \nu_\tau) < 4.9 \times 10^{-4} \text{ at the 90\% CL}$$

By combining this analysis with a statistically independent $B^+ \rightarrow \tau^+ \nu_\tau$ search performed using a semi-exclusive B reconstruction we find the preliminary combined limit:

$$\mathcal{B}(B^+ \rightarrow \tau^+ \nu_\tau)_{\text{combined}} < 4.1 \times 10^{-4} \text{ at the 90\% CL}$$

7 Acknowledgments

We are grateful for the extraordinary contributions of our PEP-II colleagues in achieving the excellent luminosity and machine conditions that have made this work possible. The success of this project also relies critically on the expertise and dedication of the computing organizations that support *BABAR*. The collaborating institutions wish to thank SLAC for its support and the kind hospitality extended to them. This work is supported by the US Department of Energy and National Science Foundation, the Natural Sciences and Engineering Research Council (Canada), Institute of High Energy Physics (China), the Commissariat à l’Energie Atomique and Institut National de Physique Nucléaire et de Physique des Particules (France), the Bundesministerium für Bildung und Forschung and Deutsche Forschungsgemeinschaft (Germany), the Istituto Nazionale di Fisica Nucleare (Italy), the Foundation for Fundamental Research on Matter (The Netherlands), the Research Council of Norway, the Ministry of Science and Technology of the Russian Federation, and the Particle Physics and Astronomy Research Council (United Kingdom). Individuals have received support from the A. P. Sloan Foundation, the Research Corporation, and the Alexander von Humboldt Foundation.

References

- [1] W.-S. Hou, Phys. Rev. D **48** (1993) 2342.
- [2] N. Cabibbo, Phys. Rev. Lett. **10**, (1963) 531.
- [3] M. Kobayashi and T. Maskawa, Prog. Th. Phys. **49**, (1972) 652.
- [4] Particle Data Group, K. Hagiwara *et al.*, Phys. Rev. **D66**, (2002) 010001.
- [5] CLEO Collaboration, T. E. Browder *et al.*, “A Search for $B \rightarrow \tau\nu$ ”, Phys. Rev. Lett. **86**, (2001) 2950.
- [6] L3 Collaboration, M Acciarri *et al.*, Phys. Lett. B **396**, (1997) 327.
- [7] ALEPH Collaboration, D. Buskulic *et al.*, Phys. Lett. B **343**, (1995) 444.
- [8] DELPHI Collaboration, P Abreu *et al.*, Phys. Lett. B **496**, (2000) 43.
- [9] *BABAR* Collaboration, B. Aubert *et al.*, Nucl. Instr. Meth. A **479**, (2002) 1.
- [10] S. Agostinelli *et al.*, “Geant4 - A Simulation Toolkit”. SLAC-PUB-9350. Submitted to Nucl. Instr. Meth. A .
- [11] *BABAR* Collaboration, B. Auber *et al.*, “A Search for $B^+ \rightarrow K^+\nu\bar{\nu}$ ”. SLAC-PUB-9309, BABAR-CONF-02-027.
- [12] G.C Fox and S. Wolfram, Phys. Rev. Lett. **75**, 785 (1995).
- [13] K. Cranmer, “Kernel Estimation in High-Energy Physics”, hep-ex/0011057.
- [14] A. L. Read, “Modified frequentist analysis of search results (the CL_s method)”, CERN-OPEN-2000-205.

- [15] *BABAR* Collaboration, B. Aubert *et al.*, “A Search for $B^- \rightarrow \tau^- \bar{\nu}$ Using a Fully Reconstructed B Sample”, *BABAR-CONF-03/004*.